Presentation at Finland Workshop 2010

March 4, 2010, Helsinki

Reconstruction of complex obstacles by singular sources of higher-order

Jijun Liu

Department of Mathematics, Southeast University
Nanjing, 210096, P.R.China
jjliu@seu.edu.cn

This is a joint-work with Dr. M.Sini at RICAM, Academy Science of Austria

Inverse scattering . . .
Reconstruction of a . . .
The efficient . . .
Numerical . . .

CONTENTS

- Part 1 Inverse scattering problems
- Part 2 Reconstruction of a complex obstacle
- Part 3 The efficient computational algorithm
- Part 4 Numerical implementations

1 Inverse scattering problems

Description of the problem

Physical configuration:

Let $D \subset \mathbb{R}^m : m = 2,3$ is an impenetrable obstacle. For given incident wave $u^i(x)$, $u(x) = u^i(x) + u^s(x)$ outside of D meets

$$\begin{cases} \Delta u + k^2 u = 0, \ x \in \mathbb{R}^m \setminus \overline{D} \\ \mathcal{B}u = 0, \ x \in \partial D \\ \lim_{r\to\infty} r^{(m-1)/2}\left(\frac{\partial u^s(x)}{\partial r} - iku^s(x)\right) = 0, \ r = |x|, \end{cases}$$

Specify the boundary operator $\mathcal{B}$:

- Sound-soft: $u|_{\partial D} = 0$
- Sound-hard:$\partial_\nu u|_{\partial D} = 0$
- Impedance boundary: $\partial_{\nu(x)} u + i\lambda u|_{\partial D} = 0$

Inverse scattering . . .
Reconstruction of a . . .
The efficient . . .
Numerical . . .

Description of the problem

Scattered wave representation:

$$u^s(x) = \frac{e^{ikr}}{r^{(m-1)/2}} \left[u^\infty(\hat{x}) + O\left(\frac{1}{r}\right)\right], \quad r \to \infty.$$

$u^\infty(\hat{x})$: far-field pattern of the scattered wave.

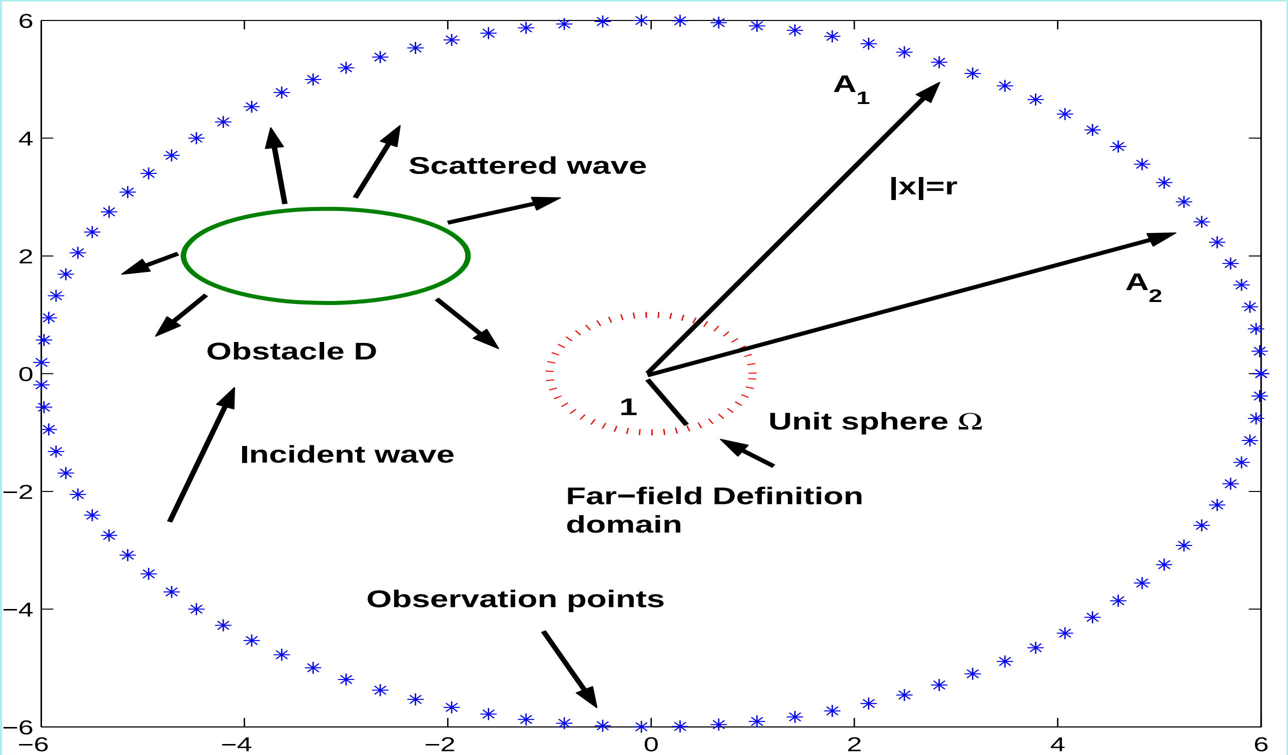

Description of the problem

Given incident plane wave $u^i(x,d) = e^{ikd\cdot x}$ for direction d.

Scattering and inverse scattering

- Direct scattering: Find scattered wave for given obstacle D.
- Inverse scattering: Detect the obstacle D from the information about u^s, including the geometric property (shape) and physical property (type/impedance).
- If D degenerates into a crack Γ, determine the shape of Γ and the physical property in both sides of Γ.

Inverse scattering . . .
Reconstruction of a . . .
The efficient . . .
Numerical . . .

2 Reconstruction of a complex obstacle

A ”complex” obstacle

By a ”complex” obstacle, we mean

- The obstacle is impenetrable and has different acoustic property at different part of ∂D, and/or
- The impedance coefficient may be complex, or
- The obstacle is a crack, with different property in its two sides.

The inverse scattering problems:

- Determine the boundary shape ∂D
- Determine the boundary type at different part of ∂D
- Determine the complex impedance coefficient

Inverse scattering . . .
Reconstruction of a . . .
The efficient . . .
Numerical . . .

Special attention:

The effect of boundary curvature and boundary impedance on the reconstruction accuracy?

We find:

- The introduction of imaginary part of boundary impedance coefficient can change the visibility of the obstacle essentially.
- The suitable distribution of boundary impedance in terms of the boundary curvature can make the obstacle more (or less) accurate.

We believe:

This observation has some potential application in some industry design problems.

Inverse scattering . . .
Reconstruction of a . . .
The efficient . . .
Numerical . . .

References

1. J.J.Liu, M.Sini, How to make an obstacle more (or less) visible from exterior measurements, submit to J. Inverse and Ill-posed Problems.

2. J.J.Liu, M.Sini, On the accuracy of the numerical detection of complex obstacles from far field data using the probe method, SIAM J. Scientific Computing, Vol.31, No.4, 2009.

3. J.J.Liu, M.Sini, Reconstruction of cracks of different types from far field measurements, to appear in Mathematical Methods in Applied Science.

4. J.J.Liu, G.Nakamura, M.Sini, Reconstruction of the shape and surface impedance from acoustic scattering data for arbitrary cylinder, SIAM J. Applied Mathematics, Vol.67, No.4, 2007.

Description of the problem

For $D \subset \mathbb{R}^2$ with $\partial D \in C^{2,1}$, assume

$$\partial D = \overline{\partial D_I} \cup \overline{\partial D_D}, \ \partial D_I \cap \partial D_D = \emptyset,$$

where ∂D_D and ∂D_I are open curves in ∂D.

For $u^i(x) = e^{i\kappa d \cdot x}$, the total wave $u(x) = u^i(x) + u^s(x)$ satisfies

$$\begin{cases} \Delta u + \kappa^2 u = 0 & \text{in } \mathbb{R}^2 \setminus \overline{D}, \\ u = 0 & \text{on } \partial D_D, \\ \dfrac{\partial u}{\partial \nu} + i\kappa\sigma u = 0 & \text{on } \partial D_I, \end{cases} \tag{1}$$

where the scattered fields u^s satisfies the Sommerfeld radiation condition.

Description of the problem

Assume that the surface impedance $\sigma(x) := \sigma^r(x) + i\sigma^i(x)$ is a Lipschitz function, $\sigma^r(x)$ has a uniform lower bound $\sigma_0^r > 0$ on ∂D_I.

∂D_I : the coated part, ∂D_D : the non-coated part.

Given $u^\infty(\cdot,\cdot)$ on $\mathbb{S}\times\mathbb{S}$, we need to

- Reconstruct ∂D;
- Reconstruct some geometrical properties of ∂D such as normal directions and the curvature;
- Distinguish ∂D_I from ∂D_D;
- Reconstruct the complex surface impedance $\sigma(x)$ on ∂D_I.

Inverse scattering . . .
Reconstruction of a . . .
The efficient . . .
Numerical . . .

Indicator function for boundary

Compared with our work in 2007, here we use the far-field data to construct the indicator directly.

probe method:

Use detecting points z outside of D to approach ∂D, consider the asymptotic behavior of the indicator.

Assume $\overline{D} \subset\subset \Omega$ for known Ω. For $a \in \Omega \setminus D$, denote by $\{z_p\} \subset \Omega \setminus \overline{D}$ a sequence tending to a. For any z_p, set D_a^p a C^2-regular domain such that $\overline{D} \subset D_a^p$ (resp. $\overline{\partial D} \subset D_a^p$) with $z_q \in \Omega \setminus \overline{D_a^p}$ for every $q = 1, 2, \cdots, p$ and that the Dirichlet interior problem on D_a^p for the Helmholtz equation is uniquely solvable.

Inverse scattering . . .
Reconstruction of a . . .
The efficient . . .
Numerical . . .

Geometric configuration of approximation domain

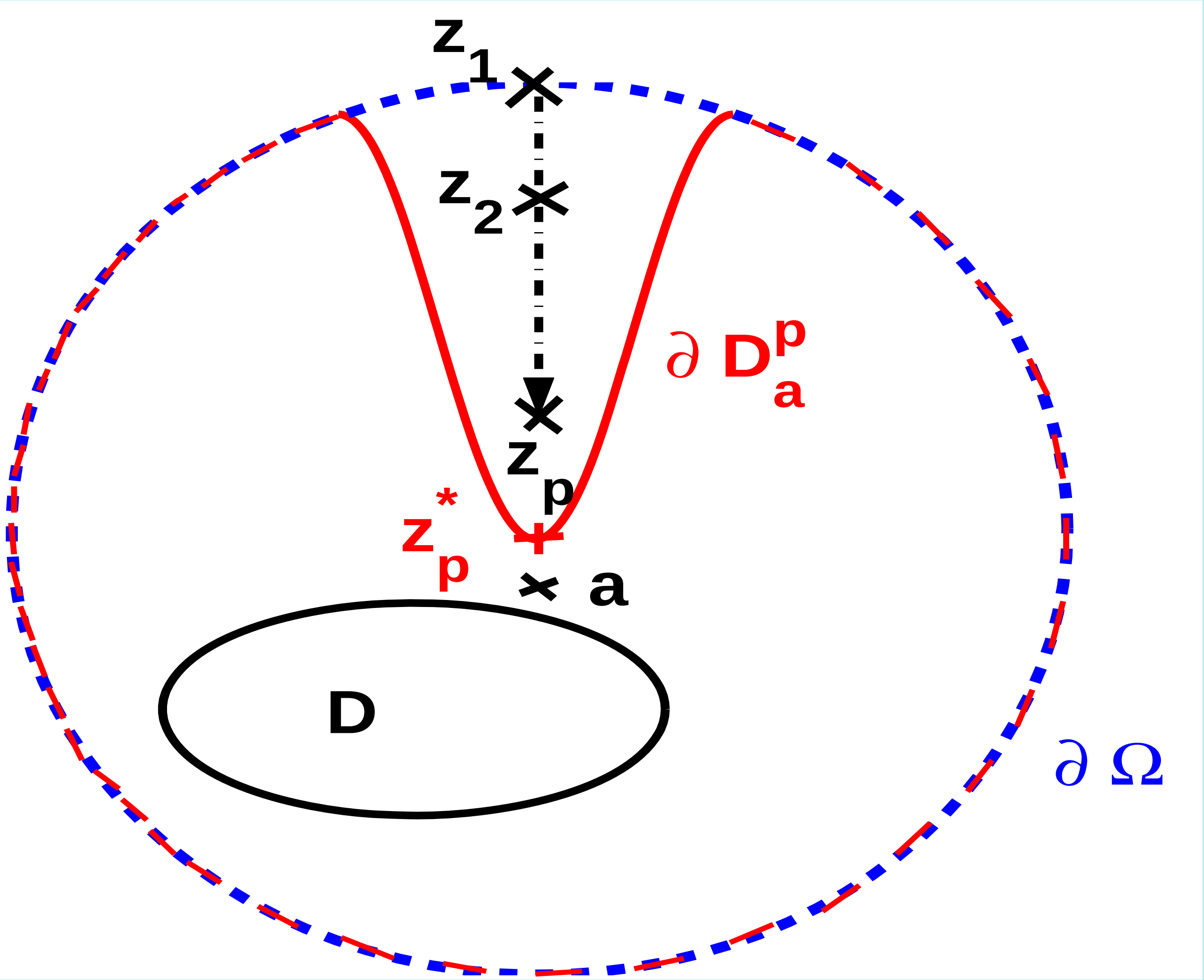

Inverse scattering . . .
Reconstruction of a . . .
The efficient . . .
Numerical . . .

Indicator function for boundary

Due to the superposition principle, the scattered field associated with the Herglotz incident field $v_g^i := v_g(x)$ defined by

$$v_g(x) := \int_{\mathbb{S}} e^{i\kappa x\cdot d} g(d)\, ds(d), \quad x \in \mathbb{R}^2 \qquad (2)$$

with $g \in L^2(\mathbb{S})$ is given by

$$v_g^s(x) := \int_{\mathbb{S}} u^s(x,d) g(d)\, ds(d), \quad x \in \mathbb{R}^2 \setminus \overline{D}, \qquad (3)$$

and its far field is

$$v_g^\infty(\hat{x}) := \int_{\mathbb{S}} u^\infty(\hat{x},d) g(d)\, ds(d), \quad \hat{x} \in \mathbb{S}. \qquad (4)$$

Inverse scattering . . .
Reconstruction of a . . .
The efficient . . .
Numerical . . .

Indicator function for boundary

In this case, the Herglotz wave operator $\mathbb{H}$ from $L^2(\mathbb{S})$ to $L^2(\partial D_a^p)$ defined by

$$\mathbb{H}[g](x) := v_g(x) = \int_{\mathbb{S}} e^{i\kappa x\cdot d} g(d)\, ds(d) \tag{5}$$

is injective, compact with dense range.

Consider the sequence of point sources: pole $\Phi(\cdot, z_p)$, dipoles $\frac{\partial}{\partial x_j}\Phi(\cdot, z_p)$ and multipoles of order two $\frac{\partial}{\partial x_j}\frac{\partial}{\partial x_2}\Phi(\cdot, z_p)$ for $j = 1, 2$, where

$$\Phi(x, y) = \begin{cases} \frac{i}{4} H_0^{(1)}(k|x-y|), & m = 2, \\ \frac{e^{ik|x-y|}}{4\pi|x-y|}, & m = 3, \end{cases}$$

is the fundamental solution.

Inverse scattering . . .
Reconstruction of a . . .
The efficient . . .
Numerical . . .

Indicator function for boundary

For every p fixed, construct three density sequences $\{g_n^p\}$, $\{f_m^{j,p}\}$ and $\{h_k^{j,p}\}$ in $L^2(\mathbb{S})$ with $j = 1, 2$, by the Tikhonov regularization such that

$$\|v_{g_n^p} - \Phi(\cdot, z_p)\|_{L^2(\partial D_a^p)} \to 0, \quad n \to \infty, \tag{6}$$

$$\|v_{f_m^{j,p}} - \frac{\partial}{\partial x_j}\Phi(\cdot, z_p)\|_{L^2(\partial D_a^p)} \to 0, \quad m \to \infty, \tag{7}$$

$$\|v_{h_k^{j,p}} - \frac{\partial}{\partial x_j}\frac{\partial}{\partial x_2}\Phi(\cdot, z_p)\|_{L^2(\partial D_a^p)} \to 0, \quad k \to \infty. \tag{8}$$

Then use these density functions to construct the indicators:

Indicator function for boundary

$$I^0(z_p) := \frac{1}{\gamma_2} \lim_{m\to\infty} \lim_{n\to\infty} \int_{\mathbb{S}} \int_{\mathbb{S}} u^\infty(-\hat{x}, d)\; g_m^p(d)\; g_n^p(\hat{x})\; ds(\hat{x}) ds(d), \tag{9}$$

$$I_j^1(z_p) := \frac{1}{\gamma_2} \lim_{m\to\infty} \lim_{n\to\infty} \int_{\mathbb{S}} \int_{\mathbb{S}} u^\infty(-\hat{x}, d)\; f_m^{j,p}(d)\; g_n^p(\hat{x})\; ds(\hat{x}) ds(d), \tag{10}$$

$$I_j^2(z_p) := \frac{1}{\gamma_2} \lim_{m\to\infty} \lim_{n\to\infty} \int_{\mathbb{S}} \int_{\mathbb{S}} u^\infty(-\hat{x}, d)\; h_m^{j,p}(d)\; g_n^p(\hat{x})\; ds(\hat{x}) ds(d), \tag{11}$$

where $\gamma_2 = e^{i\pi/4}/\sqrt{8\pi\kappa}$.

These three indicators are computable from the far-field data, and have different blowup property as $z_p \to a \in \partial D$ which make us detect the obstacle.

(Curvature $\mathcal{C}(a)$, $\sigma^i(a)$ and $\sigma^r(a)$ will enter the asymptotic behavior explicitly in our higher-order expansion of indicators!)

Inverse scattering . . .
Reconstruction of a . . .
The efficient . . .
Numerical . . .

Indicator function for boundary

Higher-order asymptotic for indicators:

I. For pole $\Phi(x, z)$ as source, it follows that

$$\Re\, I^0(z_p) = \begin{cases} -\frac{1}{4\pi} \ln |(z_p - a) \cdot \nu(a)| + O(1), & a \in \partial D_I, \\ +\frac{1}{4\pi} \ln |(z_p - a) \cdot \nu(a)| + O(1), & a \in \partial D_D. \end{cases} \tag{12}$$

$$\Im\, I^0(z_p) = O(1), \quad a \in \partial D. \tag{13}$$

II. Using dipoles $\dfrac{\partial}{\partial x_j}\Phi(x, z)$ with $j = 1, 2$ as sources, it follows that

$$\Re\, I_j^1(z_p) = \begin{cases} \frac{-\nu_j(a)}{4\pi|(z_p-a)\cdot\nu(a)|} - \frac{\nu_j(a)(\kappa\sigma^i(a)+\frac{1}{2}\mathcal{C}(a))}{\pi} \ln |(z_p - a) \cdot \nu(a)| + O(1), & a \in \partial D_I, \\ \frac{\nu_j(a)}{4\pi|(z_p-a)\cdot\nu(a)|} - \frac{\nu_j(a)}{2\pi}\mathcal{C}(a) \ln |(z_p - a) \cdot \nu(a)| + O(1), & a \in \partial D_D. \end{cases} \tag{14}$$

$$\Im\, I_j^1(z_p) = \begin{cases} -\frac{\nu_j(a)\kappa\sigma^r(a)}{\pi} \ln |(z_p - a) \cdot \nu(a)| + O(1), & a \in \partial D_I, \\ O(1), \quad a \in \partial D_D. \end{cases} \tag{15}$$

Inverse scattering . . .
Reconstruction of a . . .
The efficient . . .
Numerical . . .

Indicator function for boundary

Higher-order asymptotic for indicators:

III. Using multipoles of order two $\dfrac{\partial}{\partial x_j}\dfrac{\partial}{\partial x_2}\Phi(x,z)$ with $j=1,2$, it follows that

$$\Re\, I_1^2(z_p) = \begin{cases} \frac{\nu_1(a)\nu_2(a)}{4\pi|(z_p-a)\cdot\nu(a)|^2} - \frac{\nu_1(a)\nu_2(a)}{\pi}[\kappa\sigma^i(a) + \frac{3}{4}\mathcal{C}(a)]\frac{1}{|(z_p-a)\cdot\nu(a)|} + \\ O(\ln|(z_p-a)\cdot\nu(a)|), \quad a\in\partial D_I, \\ \frac{-\nu_1(a)\nu_2(a)}{4\pi|(z_p-a)\cdot\nu(a)|^2} - \frac{3\nu(a)_1\nu_2(a)}{4\pi}\mathcal{C}(a)\frac{1}{|(z_p-a)\cdot\nu(a)|} + \\ O(\ln|(z_p-a)\cdot\nu(a)|), \quad a\in\partial D_D. \end{cases} \tag{16}$$

$$\Re\, I_2^2(z_p) = \begin{cases} \frac{\nu_2^2(a)-\nu_1^2(a)}{8\pi|(z_p-a)\cdot\nu(a)|^2} - \frac{\nu_2^2(a)-\nu_1^2(a)}{2\pi}[\kappa\sigma^i(a) + \frac{3}{4}\mathcal{C}(a)]\frac{1}{|(z_p-a)\cdot\nu(a)|} + \\ O(\ln|(z_p-a)\cdot\nu(a)|), \quad a\in\partial D_I, \\ \frac{\nu_1^2(a)-\nu_2^2(a)}{8\pi|(z_p-a)\cdot\nu(a)|^2} - \frac{3(\nu_2^2(a)-\nu_1^2(a))}{8\pi}\mathcal{C}(a)\frac{1}{|(z_p-a)\cdot\nu(a)|} + \\ O(\ln|(z_p-a)\cdot\nu(a)|), \quad a\in\partial D_D. \end{cases} \tag{17}$$

and

$$\Im\, I_1^2(z_p) = \begin{cases} \frac{\nu_1(a)\nu_2(a)}{\pi|(z_p-a)\cdot\nu(a)|}\kappa\sigma^r + O(\ln|(z_p-a)\cdot\nu(a)|), & a\in\partial D_I, \\ O(\ln|(z_p-a)\cdot\nu(a)|), & a\in\partial D_D. \end{cases} \tag{18}$$

$$\Im\, I_2^2(z_p) = \begin{cases} \frac{\nu_2^2(a)-\nu_1^2(a)}{2\pi|(z_p-a)\cdot\nu(a)|}\kappa\sigma^r + O(\ln|(z_p-a)\cdot\nu(a)|), & a\in\partial D_I, \\ O(\ln|(z_p-a)\cdot\nu(a)|), & a\in\partial D_D. \end{cases} \tag{19}$$

Inverse scattering . . .
Reconstruction of a . . .
The efficient . . .
Numerical . . .
Home Page
Title Page
Page 18 of 49
Go Back
Full Screen
Close
Quit

Practical indicators:

Using these three indicators in a different but equivalent way, we can identify the boundary property:

Case 1. The geometric shape including the surface impedance is unknown. We can use the formula

$$\lim_{z_p \to a} \Re\, I^0(z_p) = \begin{cases} +\infty, & a \in \partial D_I, \\ -\infty, & a \in \partial D_D. \end{cases} \tag{20}$$

or

Inverse scattering . . .
Reconstruction of a . . .
The efficient . . .
Numerical . . .

Practical indicators:

$$\lim_{z_p\to a}\sum_{j=1}^{2}(\Re\, I_j^1)^2 = \begin{cases} \lim_{z_p\to a}\left[\frac{1}{16\pi^2|(z_p-a)\cdot\nu(a)|^2} - \frac{(\kappa\sigma^i+\frac{1}{2}\mathcal{C}(a))\ln|(z_p-a)\cdot\nu(a)|}{2\pi^2|(z_p-a)\cdot\nu(a)|}\right] + \\ \quad O(\frac{1}{4\pi|(z_p-a)\cdot\nu(a)|}) = +\infty,\ a\in\partial D_I, \\ \lim_{z_p\to a}\left[\frac{1}{16\pi^2|(z_p-a)\cdot\nu(a)|^2} - \frac{\mathcal{C}(a)\ln|(z_p-a)\cdot\nu(a)|}{8\pi^2|(z_p-a)\cdot\nu(a)|}\right] + \\ \quad O(\frac{1}{4\pi|(z_p-a)\cdot\nu(a)|}) = +\infty,\ a\in\partial D_D \end{cases} \tag{21}$$

$$\lim_{z_p\to a}\sum_{j=1}^{2}(\Im\, I_j^1)^2 = \begin{cases} \frac{(\kappa\sigma^r)^2}{\pi^2}\lim_{z_p\to a}\ln^2|(z_p-a)\cdot\nu(a)| + \\ \quad O(\ln|(z_p-a)\cdot\nu(a)|) = +\infty,\ a\in\partial D_I, \\ O(1),\ a\in\partial D_D \end{cases} \tag{22}$$

to detect the boundary shape.

(20) and (22) can also be used to identify the boundary type.

Our numerical performance show:
(21) is suitable for reconstructing the boundary shape, while (20) is suitable for identifying the boundary type.

Inverse scattering . . .
Reconstruction of a . . .
The efficient . . .
Numerical . . .

Practical indicators:

Detection of normal direction of ∂D:

Noticing the numerical error reconstructing ∂D, we can use the formula

$$\nu(a) = (\pm t\sqrt{\frac{1}{1+t^2}}, \pm\sqrt{\frac{1}{1+t^2}}) \text{ where } t := \lim_{z_p \to a} \frac{\Re\, I_1^1(z_p)}{\Re\, I_2^1(z_p)} = \frac{\nu_1(a)}{\nu_2(a)} \tag{23}$$

from the dipole sources to detect the normal direction, the sign $\pm$ can be fixed by the orientation of ∂D and the rough reconstruction of ∂D.

This information can be used to improve the reconstruction of ∂D.

Inverse scattering . . .
Reconstruction of a . . .
The efficient . . .
Numerical . . .

Practical indicators:

Detection of $\mathcal{C}(a)$ and $\sigma^i(a)$ in D_I:

Using the multipoles formulas, the curvature and σ^i can be computed from the known (or already computed) normal direction of ∂D. If the point a is on ∂D_I, then we start to compute the two quantities

$$\begin{aligned}\frac{3}{4}\mathcal{C}(a)+\kappa\sigma^i(a) &= -2\lim_{z_p\to a}\Big[\frac{\pi((2\nu_1(a)\nu_2(a)\Re I_1^2(z_p)+(\nu_2^2(a)-\nu_1^2(a)))\Re I_2^2(z_p))}{|(z_p-a)\cdot\nu(a)|^{-1}} \\ &\quad -\frac{1}{8|(z_p-a)\cdot\nu(a)|}\Big],\end{aligned} \tag{24}$$

$$\frac{1}{2}\mathcal{C}(a)+\kappa\sigma^i(a)=-\lim_{z_p\to a}\frac{\pi\sum_{j=1}^2\nu_j(a)\Re I_j^1(z_p)+\frac{1}{4|(z_p-a)\cdot\nu(a)|}}{\ln|(z_p-a)\cdot\nu(a)|} \tag{25}$$

from which we deduce the values of $\mathcal{C}(a)$ and $\sigma^i(a)$.

Inverse scattering . . .
Reconstruction of a . . .
The efficient . . .
Numerical . . .

Practical indicators:

Detection of $\mathcal{C}(a)$ in ∂D_D:

If a is on ∂D_D, then we have either

$$\mathcal{C}(a) = -\frac{8}{3}\lim_{z_p\to a}[\frac{\pi(2\nu_1(a)\nu_2(a)\Re I_1^2(z_p) + (\nu_2^2(a)-\nu_1^2(a))\Re I_2^2(z_p))}{|(z_p-a)\cdot\nu(a)|^{-1}} + \frac{1}{8|(z_p-a)\cdot\nu(a)|}]$$

using multipoles of order two as sources or

$$\mathcal{C}(a) = -2\lim_{z_p\to a}\frac{\pi\sum_{j=1}^{2}\nu_j(a)\Re I_j^1(z_p) - \frac{1}{4|(z_p-a)\cdot\nu(a)|}}{\ln|(z_p-a)\cdot\nu(a)|}$$

using multipoles of first order as source

Inverse scattering . . .
Reconstruction of a . . .
The efficient . . .
Numerical . . .

Practical indicators:

Detection of $\sigma^r(a)$ in ∂D_I:

$$\sigma^r(a) = -\lim_{z_p \to a} \frac{\pi \sum_{j=1}^{2} \nu_j(a) \Im\, I_j^1(z_p)}{\kappa \ln |(z_p - a) \cdot \nu(a)|}, \quad a \in D_I. \tag{26}$$

or

$$\frac{2\pi}{\kappa} \lim_{z_p \to a} \frac{2\nu_1(a)\nu_2(a) \Im\, I_1^2(z_p) + (\nu_2^2(a) - \nu_1^2(a)) \Im\, I_2^2(z_p)}{|(z_p - a) \cdot \nu(a)|^{-1}} = \sigma^r(a), a \in \partial D_I.$$

From identification to controllability

Observations:

The theoretical expression of indicators with higher order expansion contains the information about curvature and impedance simultaneously.

Numerical applications:

If the geometric shape is known/specified in advance, we can introduce suitable surface impedance distribution in terms of the curvature to adjust the blowup property of indicators.

Practical applications:

We can improve or weaken the boundary shape visibility by introducing surface impedance.

Inverse scattering . . .
Reconstruction of a . . .
The efficient . . .
Numerical . . .

The relations between curvature, $\sigma^i(x)$ and visibility

Observe

$$\sum_{j=1}^{2}(\Re\, R_j^1)^2 = \frac{1}{16\pi^2|(z_p-a)\cdot\nu(a)|^2} - \frac{(\kappa\sigma^i+\frac{1}{2}\mathcal{C}(a))\ln|(z_p-a)\cdot\nu(a)|}{2\pi^2|(z_p-a)\cdot\nu(a)|} + O(\frac{1}{4\pi|(z_p-a)\cdot\nu(a)|}) \quad (27)$$

for dipoles and

$$2\nu_1(a)\nu_2(a)\Re\, I_1^2(z_p) + (\nu_2^2(a)-\nu_1^2(a))\Re\, I_2^2(z_p) = \frac{1}{8\pi|(z_p-a)\cdot\nu(a)|^2} - \frac{\frac{3}{4}\mathcal{C}(a)+k\sigma^i(a)}{\pi|(z_p-a)\cdot\nu(a)|} + O(\ln|(z_p-a)\cdot\nu(a)|) \quad (28)$$

for multipoles.

Conclusion:

If we take $\partial D \equiv \partial D_I$ and choose $\sigma^i(x)$ such that $(\kappa\sigma^i + \frac{1}{2}\mathcal{C}(a))$ (respt. $\frac{3}{4}\mathcal{C}(a) + k\sigma^i(a)$) is uniformly distributed, then ∂D is easily detected.

Inverse scattering . . .
Reconstruction of a . . .
The efficient . . .
Numerical . . .

3 The efficient computational algorithm

Main task in recovering ∂D

Recall the indicator:

$$I^0(z_p) := \frac{1}{\gamma_2} \lim_{m\to\infty} \lim_{n\to\infty} \int_{\mathbb{S}^1}\int_{\mathbb{S}^1} u^\infty(-\hat{x}, d)\, g_m^p(d)\, g_n^p(\hat{x})\, ds(\hat{x}) ds(d), \tag{29}$$

$$I_j^1(z_p) := \frac{1}{\gamma_2} \lim_{m\to\infty} \lim_{n\to\infty} \int_{\mathbb{S}^1}\int_{\mathbb{S}^1} u^\infty(-\hat{x}, d)\, f_m^{j,p}(d)\, g_n^p(\hat{x})\, ds(\hat{x}) ds(d), \tag{30}$$

$$I_j^2(z_p) := \frac{1}{\gamma_2} \lim_{m\to\infty} \lim_{n\to\infty} \int_{\mathbb{S}^1}\int_{\mathbb{S}^1} u^\infty(-\hat{x}, d)\, h_m^{j,p}(d)\, g_n^p(\hat{x})\, ds(\hat{x}) ds(d), \tag{31}$$

and

$$\|v_{g_n^p} - \Phi(\cdot, z_p)\|_{L^2(\partial D_a^p)} \to 0, \quad n \to \infty, \tag{32}$$

$$\|v_{f_m^{j,p}} - \frac{\partial}{\partial x_j}\Phi(\cdot, z_p)\|_{L^2(\partial D_a^p)} \to 0, \quad m \to \infty, \tag{33}$$

$$\|v_{h_k^{j,p}} - \frac{\partial}{\partial x_j}\frac{\partial}{\partial x_2}\Phi(\cdot, z_p)\|_{L^2(\partial D_a^p)} \to 0, \quad k \to \infty, \tag{34}$$

where

$$v_g(x) := \mathbb{H}[g](x) = \int_{\mathbb{S}^1} e^{i\kappa x\cdot d} g(d)\, ds(d) \tag{35}$$

Inverse scattering . . .
Reconstruction of a . . .
The efficient . . .
Numerical . . .

Recall the approximation domain

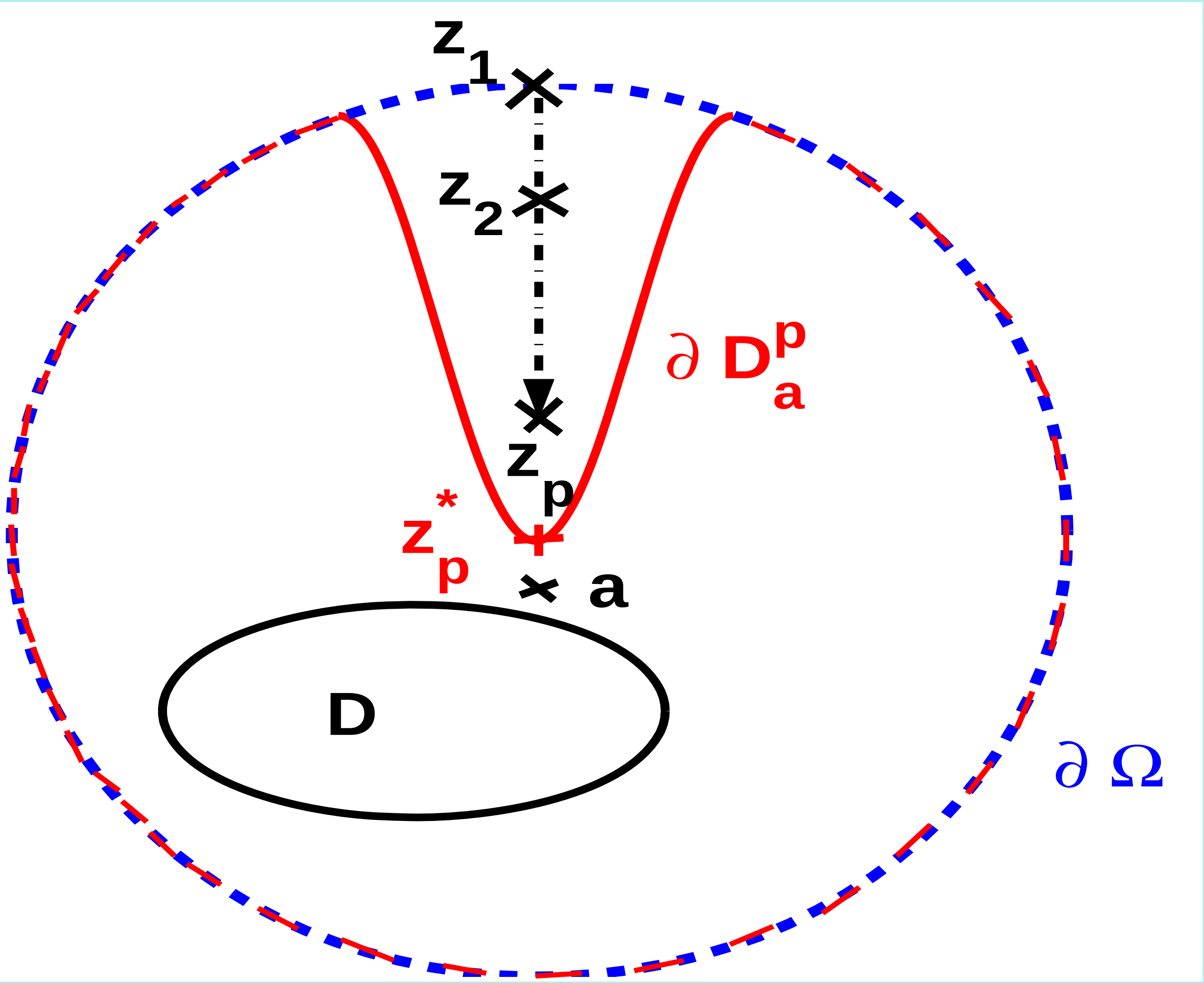

Inverse scattering . . .
Reconstruction of a . . .
The efficient . . .
Numerical . . .

Compute the three density functions

To reconstruct ∂D, we should compute $g_m^p(d), f_m^{j,p}(d), h_m^{j,p}(d)$ for $z_p \to a$ with all possible a around ∂D, large amount of computations!

Hope: When a rotates around ∂D, the approximate domain D_a^p also rotates!

Solution:

- Generate D_a^p from some fixed domain D_0;
- Approximate the singular sources in ∂D_0 using the minimum norm solution $g_0(d), f^{j,0}(d), h^{j,0}(d)$ for $0 \notin D_0$.
- Generate $g_m^p(d), f_m^{j,p}(d), h_m^{j,p}(d)$ for $z_p \to a$ from $g_0(d), f^{j,0}(d), h^{j,0}(d)$ by some simple ways and guarantee the approximate relations!

Compute the three density functions

Known work by Potthast in 2000:
For reference domain G_0 with $0 \notin G_0$, let

$$G := \mathbb{M}G_0 + z_0,$$

with an orthogonal unit matrix $\mathbb{M}$ and vector z_0: G is generated from G_0 by rotation and translation!
Consider two integral equations of the first kind

$$\mathbb{H}[g_0](x) = \Phi(x, 0), \quad x \in \partial G_0, \tag{36}$$
$$\mathbb{H}[g](x) = \Phi(x, z_0), \quad x \in \partial G. \tag{37}$$

Result: Assume that $g_0(d)$ is the MNS of (36) with discrepancy ε. Then

$$g(d) := g_0(\mathbb{M}^{-1}d)e^{-i\kappa d\cdot z_0} \tag{38}$$

is MNS of (37) with discrepancy $\varepsilon > 0$.

Inverse scattering . . .
Reconstruction of a . . .
The efficient . . .
Numerical . . .

Compute the three density functions

Importance:

- Only compute the MNS of (36) once in ∂G_0;
- $g(d)$ can be computed in a simple way;
- $g(d)$ is also the MNS of (37);
- The approximation in ∂G is also ε.

Our problems: How to approximate dipole $\Phi_{x_j}(x, z_0)$ and multipoles $\Phi_{x_j x_2}(x, z_0)$ for $j = 1, 2$?

For $(\varphi_1, \varphi_2)^T \in L^2(\mathbb{S}) \times L^2(\mathbb{S})$, define

$$\mathbb{H}[(\varphi_1, \varphi_2)^T](x) := (\mathbb{H}[\varphi_1](x), \mathbb{H}[\varphi_2](x))^T.$$

For functions $(f_1, f_2)^T \in L^2(\Gamma) \times L^2(\Gamma)$, define

$$\|(f_1, f_2)^T\|^2_{L^2(\Gamma\times\Gamma)} := \|f_1\|^2_{L^2(\Gamma)} + \|f_2\|^2_{L^2(\Gamma)}.$$

Inverse scattering . . .
Reconstruction of a . . .
The efficient . . .
Numerical . . .

Compute the three density functions

We have the following generalizations:

Result 1: Assume that $f_0^j(d)$ with $j = 1, 2$ are MNS of

$$\mathbb{H}[f_0^j](x) = \Phi_{x_j}(x, 0), \quad x \in \partial G_0 \tag{39}$$

with discrepancy $\varepsilon > 0$. Then $(f^1, f^2)^T$ given by

$$\begin{pmatrix} f^1(d) \\ f^2(d) \end{pmatrix} := \mathbb{M} \begin{pmatrix} f_0^1(\mathbb{M}^{-1}d) \\ f_0^2(\mathbb{M}^{-1}d) \end{pmatrix} e^{-i\kappa d\cdot z_0} \tag{40}$$

satisfies that

$$\|\mathbb{H}[(f^1, f^2)^T](\tilde{x}) - (\Phi_{\tilde{x}_1}, \Phi_{\tilde{x}_2})^T(\tilde{x}, z_0)\|^2_{L^2(\partial G)} \le 2\varepsilon^2. \tag{41}$$

Inverse scattering ...

Reconstruction of a ...

The efficient ...

Numerical ...

Compute the three density functions

Result 2: Assume that $h_0^j(d)$ with $j=1,2$ are MNS of

$$\mathbb{H}[h_0^j](x) = \Phi_{x_j x_2}(x,0), \quad x \in \partial G_0 \tag{42}$$

with discrepancy $\varepsilon > 0$. Then $(h^1, h^2)^T$ given by

$$\begin{pmatrix} h^1(d) \\ h^2(d) \end{pmatrix} := \mathbb{M}^2 \begin{pmatrix} h_0^1(\mathbb{M}^{-1}d) \\ h_0^2(\mathbb{M}^{-1}d) \end{pmatrix} e^{-i\kappa d\cdot z_0} - \mathbb{M} \begin{pmatrix} \kappa^2 m_{21} \\ 0 \end{pmatrix} g(\mathbb{M}^{-1}d) e^{-i\kappa d\cdot z_0} \tag{43}$$

satisfies that

$$\|\mathbb{H}[(h^1,h^2)^T](\cdot) - (\Phi_{\tilde{x}_1\tilde{x}_2}, \Phi_{\tilde{x}_2\tilde{x}_2})^T(\cdot, z_0)\|^2_{L^2(\partial G)}$$
$$\leq (2+\kappa^2)\varepsilon^2. \tag{44}$$

Compute the three density functions

Using this result, we can approximate the singular sources by Herglotz wave functions in all approximate domains $\partial D_a^p := \mathbb{M}(a)D_0 + z_p$ with a few amount of computations.

- $\mathbb{M}(a)$: approaching direction and z_p : approaching step along this direction.
- Choose different $\mathbb{M}(a)$ and z_p from D_0, $z_p \notin D_a^p$ can approach to any points $a \in \partial D$.
- We compute MNS φ_0 in ∂D_0, the density functions for approaching singular source in ∂D_a^p can be computed from φ_0 by a simple function transformation.

Inverse scattering . . .
Reconstruction of a . . .
The efficient . . .
Numerical . . .

Configuration of G_0 with some cone shape boundary and its transform

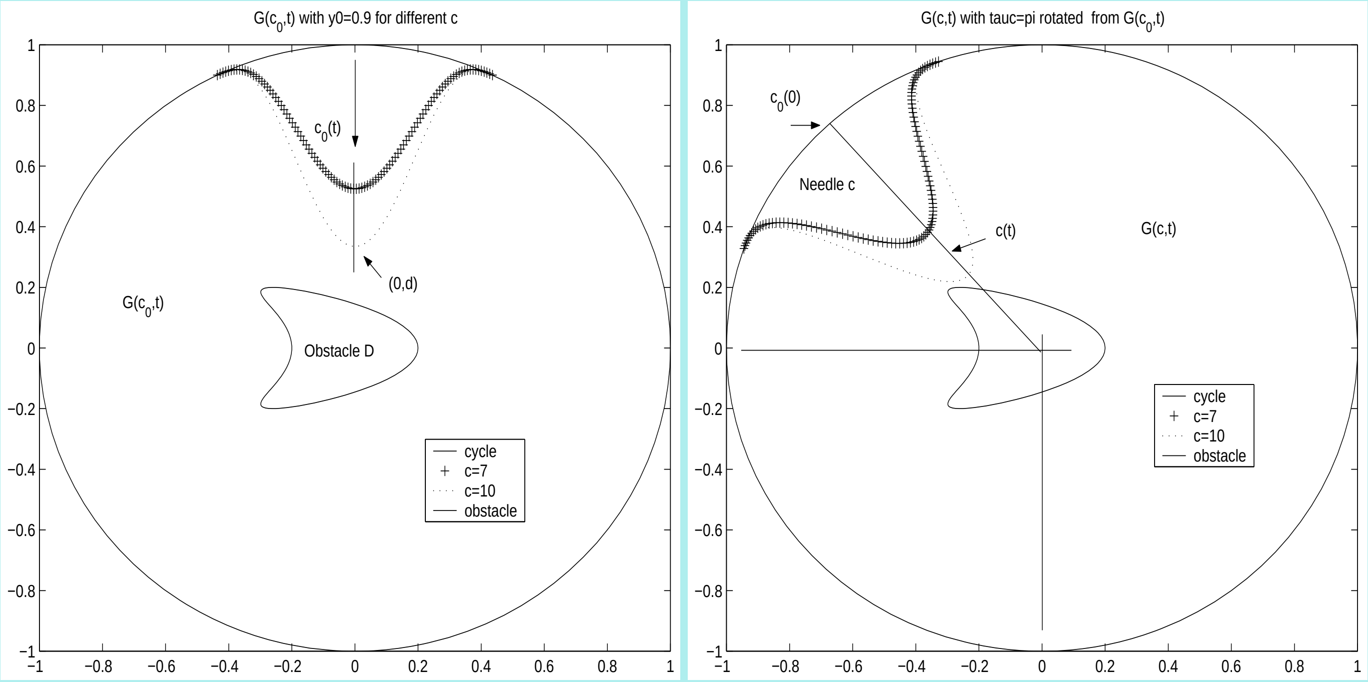

Inverse scattering . . .
Reconstruction of a . . .
The efficient . . .
Numerical . . .

Special Difficulty

The essences of approximating $\Phi(x, z_0)$ (respt. $\Phi_{x_j}(x, z_0), \Phi_{x_1 x_j}(x, z_0)$) by Herglotz wave function

$$\mathbb{H}[g] := \int_{\mathbb{S}^1} e^{i\kappa x\cdot d} g_{z_0}(d) ds(d)$$

in ∂G for z_0 near to ∂G is: Approximate a almost singular function by a smooth function.

Notice: Real part of Φ is almost singular, while its imaginary part is smooth.

Difficulty:

- Integral equation of the first kind;
- The right-hand side is almost singular;
- Efficient solution algorithm.

Inverse scattering . . .
Reconstruction of a . . .
The efficient . . .
Numerical . . .

Approximation behavior:

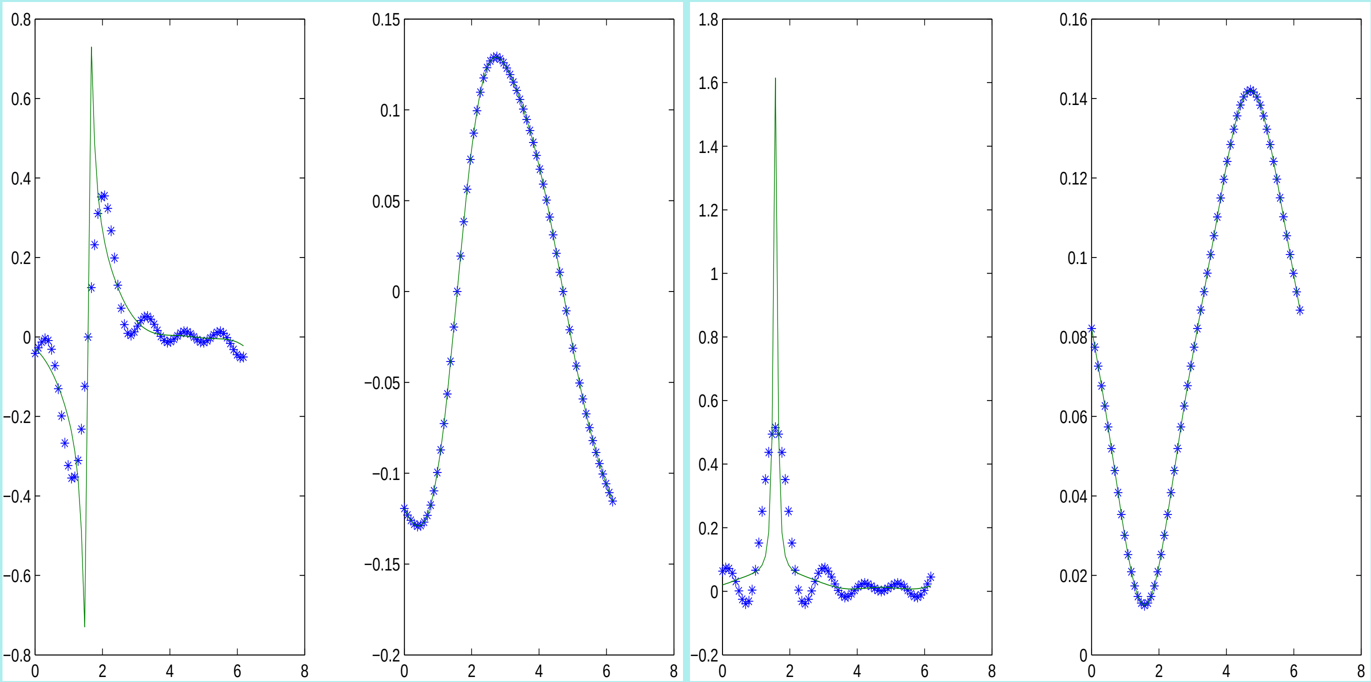

The singular behaviors of $\Phi_{x_1}(x, z_0)$ (left) and $\Phi_{x_2}(x, z_0)$ (right) in a circle $|x| = R_0$ with $z_0 = (0, R_0 + \delta_0)$ for small δ_0, together with their approximations shown in star line using uniform mesh.

Inverse scattering . . .
Reconstruction of a . . .
The efficient . . .
Numerical . . .

4 Numerical implementations

Model problem

We focus on the effect of surface impedance and the obstacle curvature, by using (21) to detect the boundary, explaining the effect of surface impedance.

Example 1. Take $\kappa = 1, 2$ and D being a cycle

$$\partial D := \{x = 1.5 \times (\cos t, \sin t), t \in [0, 2\pi]\}.$$

Case 1: The surface impedance is a real constant, ∂D has a mixed boundary

$$\partial D_D = \{x \in \partial D : t \in [0, \pi)\}, \quad \partial D_I = \{x \in \partial D : t \in (\pi, 2\pi]\}$$

The results for $\sigma(x) = 30, \sigma(x) = 3$ using the same criterion in all directions are shown below.

Inverse scattering . . .
Reconstruction of a . . .
The efficient . . .
Numerical . . .

Numerics:

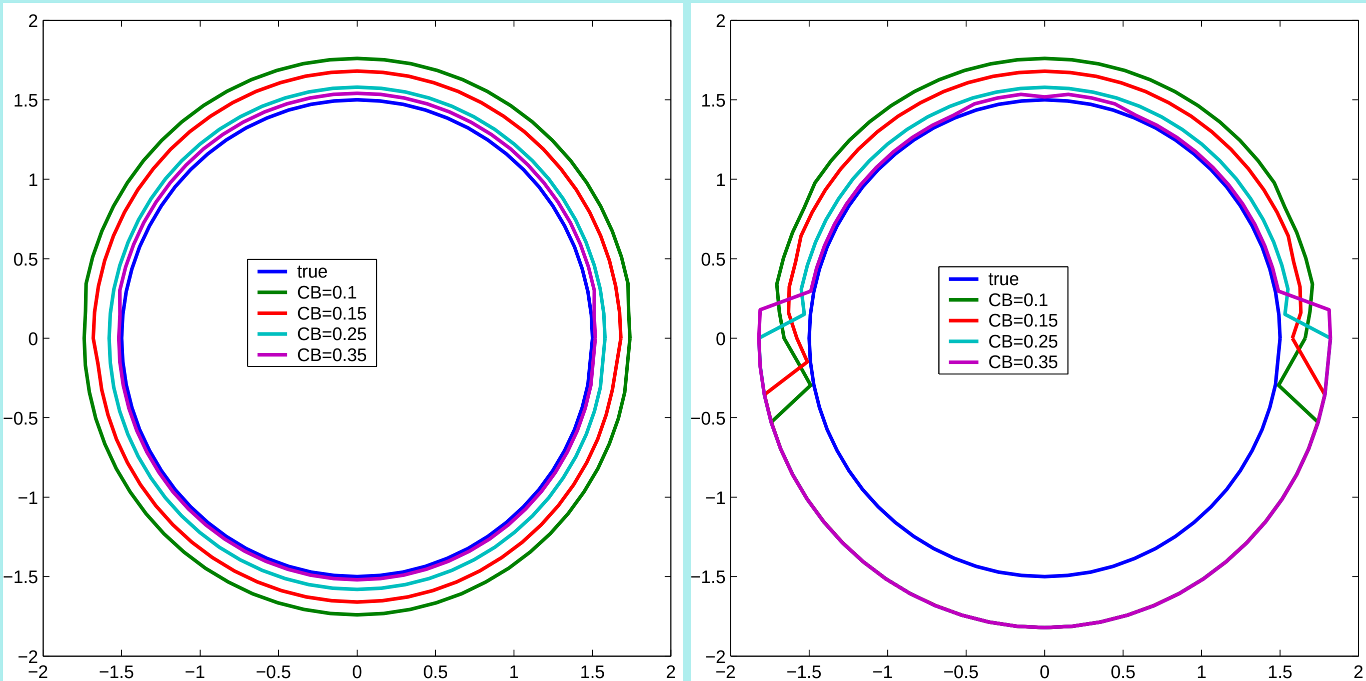

Recovery of ∂D for mixed boundary condition with $\sigma(x) = 30$ (left) and $\sigma(x) = 3$ (right).
For small $\sigma(x)$ (right), the blowing-up behavior for the impedance boundary is weak. Using the same criterion in all directions, the impedance part can not be detected (just initial guess).

Inverse scattering . . .
Reconstruction of a . . .
The efficient . . .
Numerical . . .

Numerics:

Case 2: The surface impedance case.
We assume $\partial D = \partial D_I$ and consider three cases:

$$\sigma(x) = 5-5i, \sigma(x) = 5-\frac{0.6667}{2\kappa}i, \sigma(x) = 5-5\sin(6x_1x_2)i.$$

The second case meets $\frac{1}{2}\mathcal{C}(a) + \kappa\sigma^i(a) \equiv 0$ in ∂D_I.

Using different uniform blowing-up values, the reconstructions are given below for the first two configurations. We see that the whole obstacle can be seen for both cases. However, the reconstruction is better in the picture of the left hand side.

This is natural and it can be explained using (27).

Inverse scattering . . .
Reconstruction of a . . .
The efficient . . .
Numerical . . .

Numerics:

Reconstruction in the first two-cases.

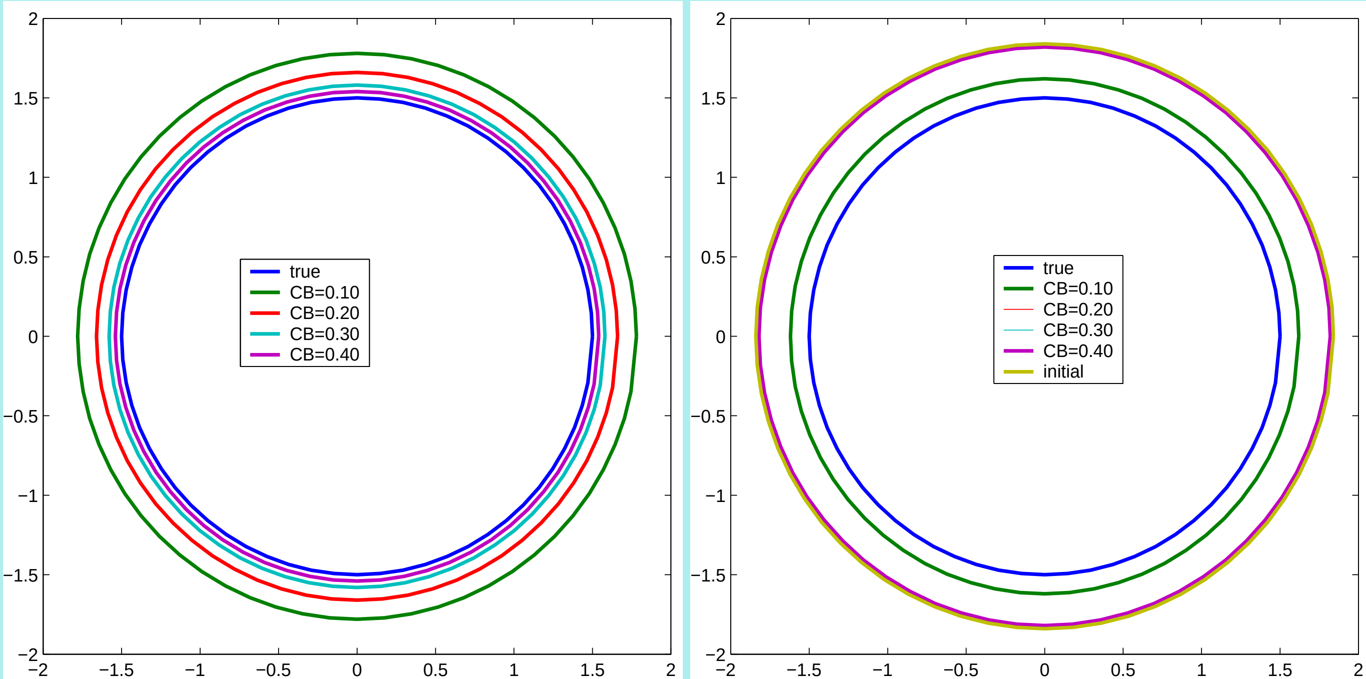

Reconstruction of ∂D for surface impedance in ∂D with $\sigma(x) = 5 - 5i$ (left) and $\sigma(x) = 5 - \frac{0.6667}{2\times 1.2} i$ (right), using the uniform blowing-up criteria in all directions. For large blowing-up values, the boundary can not be seen (right).

Inverse scattering . . .
Reconstruction of a . . .
The efficient . . .
Numerical . . .

Numerics:

Case 2: The surface impedance case.
In the third configuration, the imaginary part of impedance has serious oscillation.

It can be seen that the oscillation of $\sigma^i(x)$ on ∂D makes the reconstruction of the obstacle less accurate. In addition, for large blowing-up values of CB, we cannot recognize at all the very well uniform shape of a circle. It is worth noticing that this phenomenon should be the same using any of the indicator functions I^0, I^i_j, $i, j = 1, 2$ or even using of indicators based on multipoles of higher orders.

Inverse scattering . . .
Reconstruction of a . . .
The efficient . . .
Numerical . . .

Numerics:

Reconstruction in the third configuration.

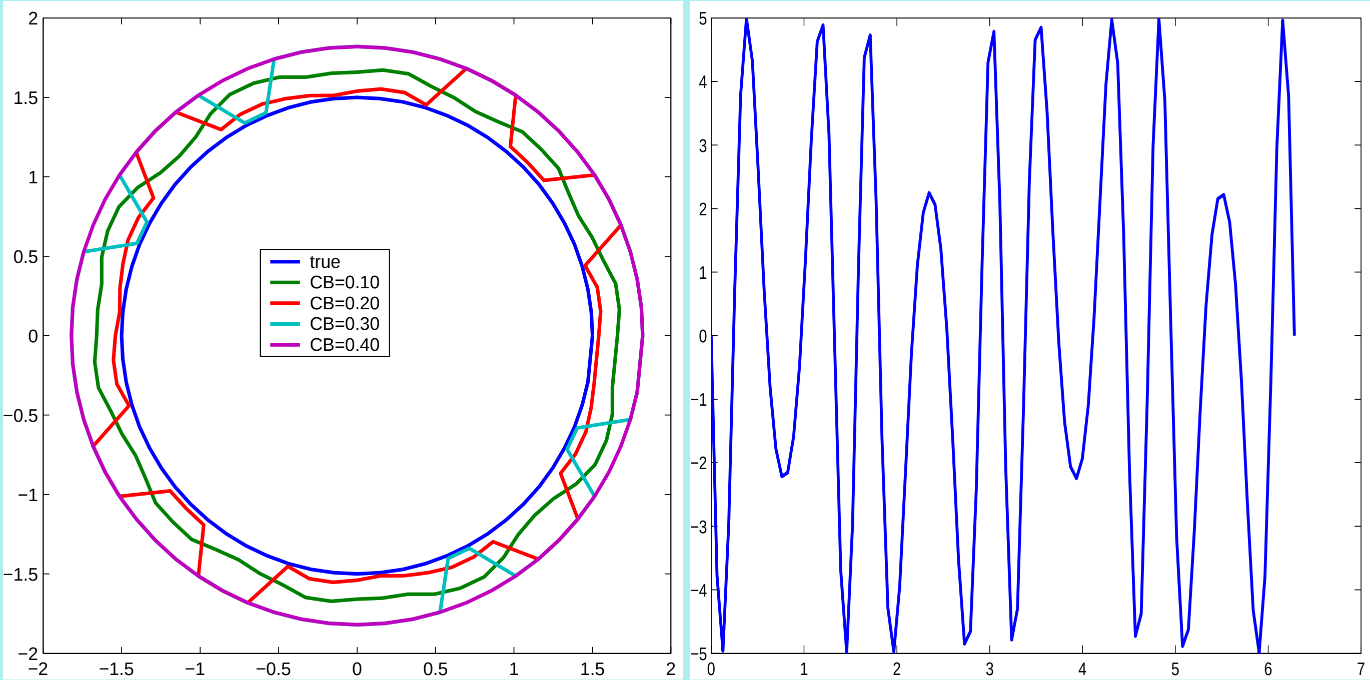

Reconstruction of ∂D for surface impedance with oscillatory imaginary part(left), and the function $\Im\, \sigma(x)$(right). The formula (21) can be used to explain this reconstruction. That is, the oscillation of $\sigma^i(x)$ in ∂D_I decreases the visibility of obstacle.

Inverse scattering . . .
Reconstruction of a . . .
The efficient . . .
Numerical . . .

Numerics:

Example 3. Consider a complex obstacle

$$\partial D = \{x : x(t) = (\cos t + 0.65\cos 2t - 0.65, 1.5\sin t), t \in [0, 2\pi]\},$$

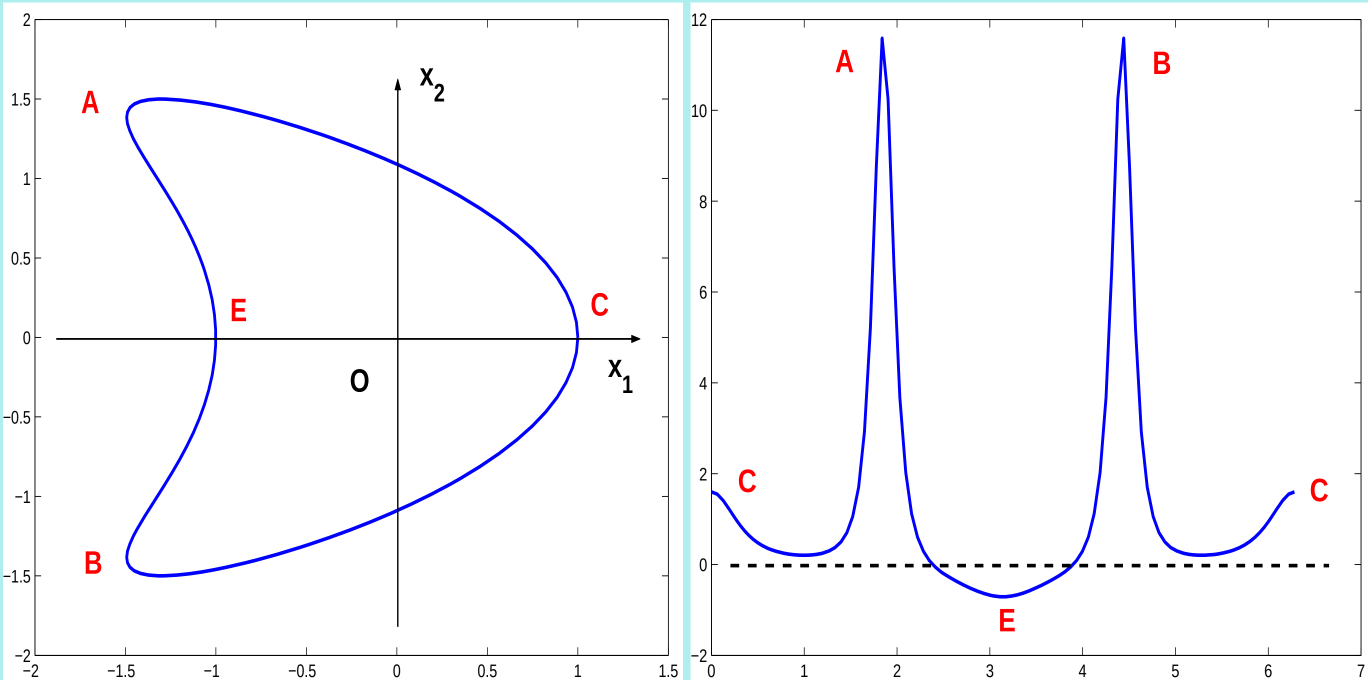

A kite-shaped obstacle (left) and its curvature distribution with respect to the polar angle (right). The curvature takes maximum value near points A, B, which means a strong scattering in this part.

Inverse scattering . . .
Reconstruction of a . . .
The efficient . . .
Numerical . . .

Numerics:

Case 1. Consider the constant surface impedance for $\sigma(x) = 5, \sigma(x) = 5 - 5i$.

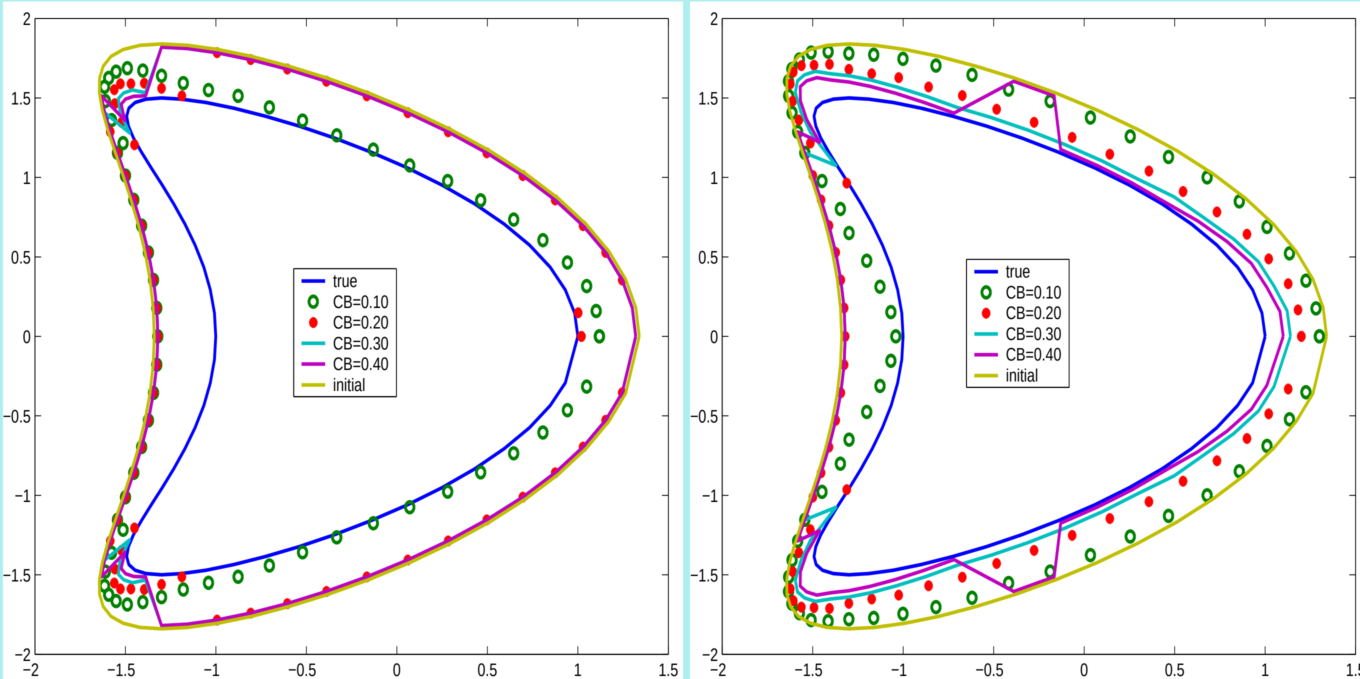

For real surface impedance, the part of the boundary with the maximum curvature is relatively easy to be detected. For $\sigma(x) \equiv 5 - 5i$ with blowup value $CB = 0.4$, the reconstruction is not improved for the part with minimum absolute value of curvature, due to the constant imaginary part.

Inverse scattering . . .
Reconstruction of a . . .
The efficient . . .
Numerical . . .

Numerics:

Case 2. Curvature effect.

Take $\sigma(x) = 5 + \sigma^i(x)i$. The reconstructions with $\sigma^i(x)$ satisfying $\frac{1}{2}\mathcal{C}(x) + \kappa\sigma^i(x) \equiv -5$ (left) and $\frac{1}{2}\mathcal{C}(x) + \kappa\sigma^i(x) \equiv -10$ (right) in ∂D are shown below.

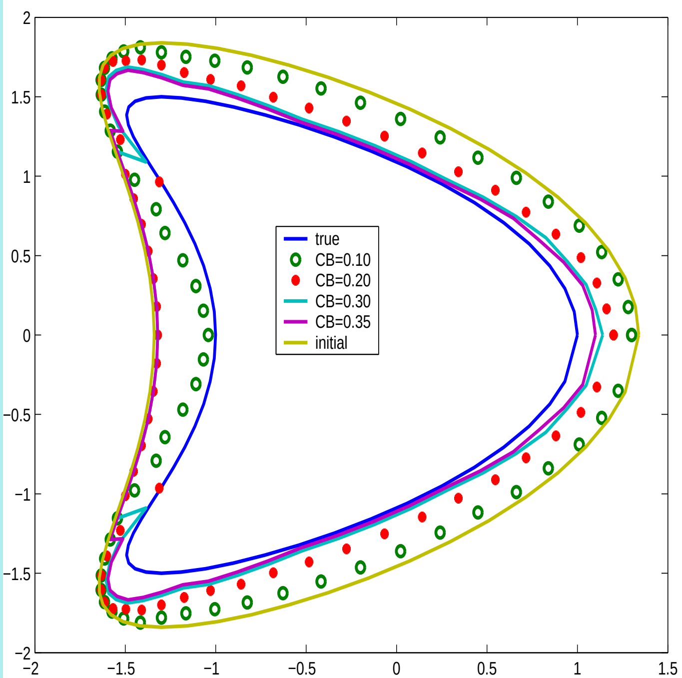

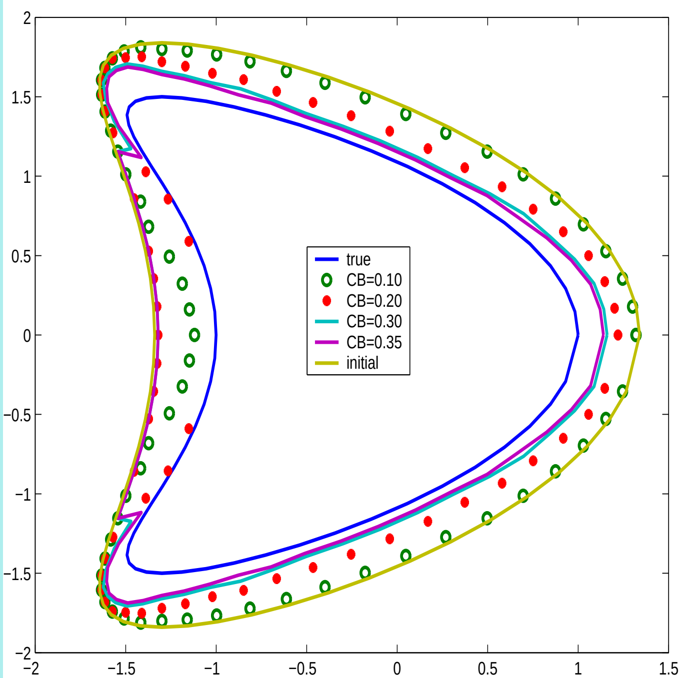

Inverse scattering . . .
Reconstruction of a . . .
The efficient . . .
Numerical . . .

Observations:

The variable imaginary part of impedance in terms of the curvature removes the nonuniform blowing-up due to the curvature distribution.

Explanation:

- The uniform blowing-up property is obtained, except on the parts near the point E, where the curvature takes the negative minimum value.
- This phenomena is physically reasonable. There are multiple reflections of the scattered wave. So the information about this concave side is relatively small in the far-field data.
- To explain more about this phenomenon, a higher asymptotic expansion using higher multipole sources is needed.

Inverse scattering . . .
Reconstruction of a . . .
The efficient . . .
Numerical . . .

Some open problems:

- Efficient realization of singular sources approximation;
- Numerically reconstruction of boundary impedance by asymptotic expression;
- Physical explanation on $\Im\sigma(x) \neq 0$?
- Convergence order analysis for noisy data $u_\delta^\infty(\hat{x}, d)$?
- 3-dimensional obstacle case?
- Potential applications?

Inverse scattering . . .
Reconstruction of a . . .
The efficient . . .
Numerical . . .

Thanks a lot !

Inverse scattering . . .
Reconstruction of a . . .
The efficient . . .
Numerical . . .